Infrared lines as probes of solar magnetic features

XIV. Ti I and the cool components of sunspots

I. Rüedi[1], S.K. Solanki[1], C.U. Keller[2], and C. Frutiger[1]

[1] Institute of Astronomy, ETH–Zentrum, CH-8092 Zürich, Switzerland
[2] National Solar Observatory, NOAO[*], P.O. Box 26732, Tucson, AZ 85726, USA

Abstract. The first systematic observations of sunspot umbrae using the lines of the Ti I multiplet at 2.2 μm are presented. Their diagnostic capabilities are investigated, developed and used to investigate the magnetic and velocity structure of a sunspot. These lines are most sensitive to cool plasma. In addition, they are extremely Zeeman sensitive. We find that a sunspot is composed of two distinct cool magnetic components. One of them is fairly vertical, has a large magnetic field strength and is associated with the central (umbral) part of the sunspot. The other component is strongest near the outer boundary of the spot (penumbra), is much more inclined, has a very low magnetic field strength and shows the signature of the Evershed effect. In contrast to the smooth transition of field strength from the darkest part of the umbra to the outer penumbral boundary usually visible in observations carried out in other spectral lines, the Ti I lines exhibit a sharp transition between the two magnetic components.

1. Introduction

The observation of umbral magnetic field strengths is, on the one hand, simple since the strong umbral field completely splits Zeeman sensitive spectral lines. On the other hand, such measurements are hampered by a number of factors. For example, the low umbral temperature leads to a strengthening of profiles due to neutral species, i.e. to their saturation and hence broadening, which partly cancels the advantage of the large field strength, and can result in large uncertainties in the measured field strengths. Another problem is due to contamination by stray-light from the surrounding penumbra and plages, which can corrupt even polarized line profiles and lead to errors in the deduced strength and inclination of the magnetic vector. A final problem arises from blending by purely umbral (e.g. molecular)

Table 1. Titanium multiplet: atomic parameters

Ion	λ [Å]	Transition	$g_{\rm eff}$	χ_e [eV]	$\log gf$
Ti I	22310.61	$a\ ^5P_1 - z\ ^5D_0^\circ$	2.500	1.73	−2.21
Ti I	22211.22	$a\ ^5P_1 - z\ ^5D_1^\circ$	2.000	1.73	−1.85
Ti I	22232.91	$a\ ^5P_2 - z\ ^5D_2^\circ$	1.667	1.74	−1.74
Ti I	22274.07	$a\ ^5P_3 - z\ ^5D_3^\circ$	1.583	1.75	−1.84
Ti I	21897.38	$a\ ^5P_2 - z\ ^5D_3^\circ$	1.167	1.74	−1.53

lines, which distorts the profiles of a number of Zeeman sensitive spectral lines (e.g. the $g = 3$ Fe I line at 1.5648 μm, as shown for example in Fig. 5 of Solanki et al. 1992a).

The lines of the Ti I multiplet at 2.2 μm are not affected by any of these problems and are therefore ideal candidates for stray-light free measurements of umbral magnetic fields. These lines have so far not been used for the investigation of solar magnetic structures, although they have previously been observed in sunspots (Hall 1974, Wallace & Livingston 1992, Rüedi et al. 1995) and have been employed to probe the magnetic field of late-type stars (Saar & Linsky 1985, Saar 1996a, b). In this paper we report on the first systematic scans through a sunspot using these lines, as well as the first numerical transfer calculations of these lines. The observations and their inversions demonstrate some of the lines' potential as magnetic field diagnostics.

The structure of this paper is as follows. First, in Sect. 2, we present the spectral lines and their properties. Sect. 3 describes the observations and Sect. 4 the manner in which we correct the data for telluric line blending. The analysis and the results are presented in Sects. 5 and 6. Finally, the main findings are discussed in Sect. 7 and summarized in Sect. 8.

2. Spectral line characteristics

The Ti I lines treated in this paper all belong to the same multiplet. The wavelengths, transitions, effective Landé factors, $g_{\rm eff}$, excitation potentials, χ_e, and logarithmic oscillator strengths, $\log gf$ (Biémont 1976), of all the lines in this multiplet are listed in Table 1.

2.1. Magnetic sensitivity

The combination of long wavelengths and large Landé factors makes some of the Ti I lines extremely sensitive to magnetic fields. For example, consider the product $g\lambda$, which is a measure of the Zeeman sensitivity of a line. For the Zeeman triplet, Ti I 22310 Å, it is 5.6, which compares favourably with the value of 4.7 found for the already extremely sensitive Fe I 15648 Å line. The Zeeman splitting of this Ti I line can on its own give precise field strength values in umbrae and penumbrae. Furthermore, the simultaneous use of two of these lines, having different Landé factors, provides an additional diagnostic of magnetic field strength distributions.

The Zeeman sensitivities of these lines are sufficiently large that umbral observations can begin to distinguish not just between their Landé factors, but also between their Zeeman splitting patterns.

2.2. Splitting patterns

Fig. 1 shows the splitting patterns of the lines of the Ti I multiplet at 2.2 μm (transverse Zeeman effect). The first line (Ti I 22310 Å) is the only Zeeman triplet of the multiplet. The horizontal axis gives the line splitting in mÅ/G. The vertical bars represent the relative intensities of each component normalized such that the sum of all components is unity. The π- and σ-components are plotted above and below the horizontal line, respectively. These splitting patterns should be compared with the line profiles plotted in Fig. 5. For example, the two pairs of σ-components of Ti I 22211 Å are clearly seen in both its Stokes I and V profiles, while its π-component contributes marginally to the inner flanks of the Stokes I profile. Their very low intensity is due to the fairly longitudinal orientation of the magnetic field vector sampled by the Stokes profiles in this figure. The split π-component is very clearly seen in the Stokes Q profiles in Figs. 6 and 7.

2.3. Heights of formation

Fig. 2a shows the Stokes I profiles of Ti I 22310 Å computed using the radiative model of Kurucz (1991a, b) with effective temperature $T_{\text{eff}} = 4250$ K, a magnetic field strength of 2000 G and no macroturbulent velocity broadening. Clearly the two σ-components are very well separated. Fig. 2b shows the line depression contribution function surface (Grossmann-Doerth et al. 1988) corresponding to this line profile as a function of wavelength and continuum optical depth (at 22000 Å) in the atmosphere. In Fig. 2c a cut through this surface at the wavelength of the Stokes I intensity minimum is plotted as a function of geometrical height. For comparison purposes similar curves have been plotted for other magnetically sensitive lines which are frequently used for sunspot investigations. (The other lines of the Ti I multiplet have similar contribution functions as the triplet at 22310 Å.) For the considered atmosphere the contribution function of the Ti I line peaks at 110 km and has a half-width of 140 km. The Fe I 15648 Å line is formed much lower in the
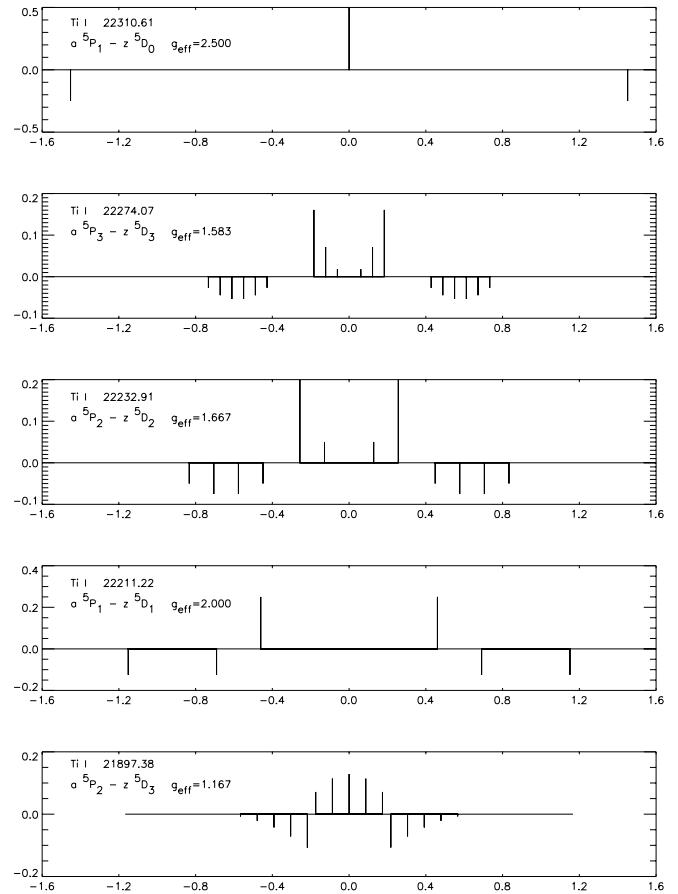

Fig. 1. Zeeman splitting patterns of the Ti I multiplet lines in mÅ/G. The relative intensity of the different line components are plotted vertically. The π-components are represented by positive values while the σ-components are represented by negative values.

atmosphere (its contribution has a maximum at 20 km) and over a much narrower height range (70 km), while the Fe I 6302 Å line is formed higher (150 km) and over a similarly large height range (130 km). Although the exact numbers depend on the detailed definition of the contribution function, and are somewhat different if instead response functions are calculated, some features are nevertheless robust. These include that the Ti I lines are formed between the Fe I 15648 Å and Fe I 6302 Å lines and that the height range sampled by the Ti I lines overlaps those sampled by the other two lines, in particular Fe I 6302 Å.

2.4. Temperature sensitivity

The unique diagnostic value of these lines stems not just from their large Zeeman sensitivity, but also from their temperature sensitivity. To explore this we need to carry out accurate radiative transfer calculations. At umbral temperatures a portion of the Ti atoms is bound into TiO molecules, so that the strength of atomic Ti I lines is reduced. In order to take this effect properly into account, we have incorporated the molecular dissociation equilibrium (Mihalas 1967) into the employed radiative transfer code (Solanki 1987, Solanki et al. 1992a).
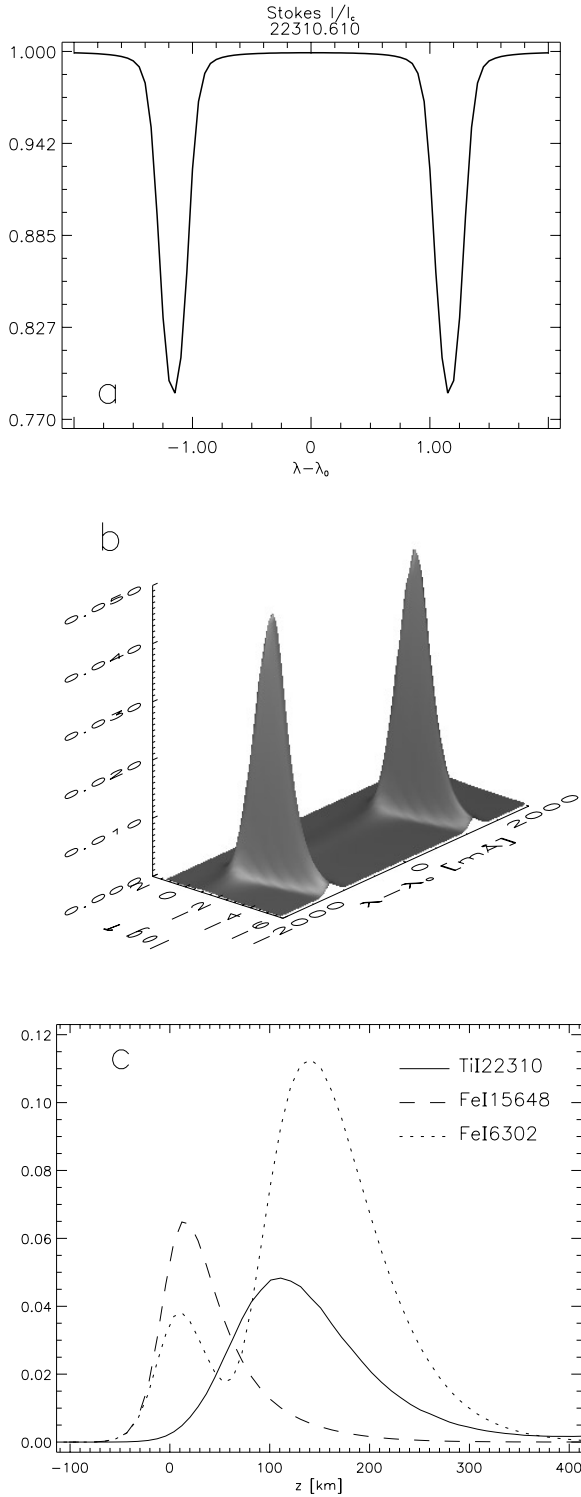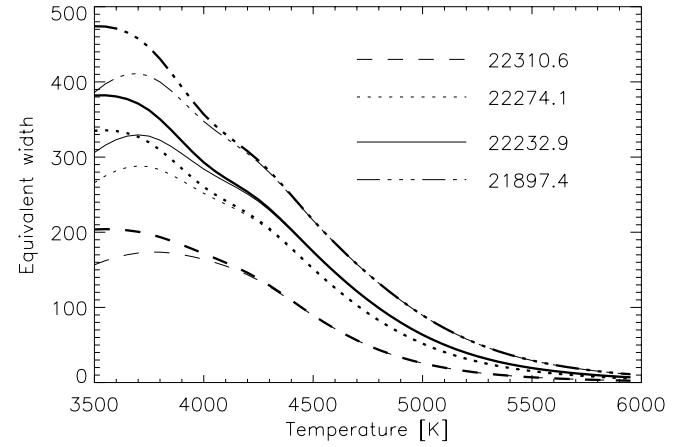
Fig. 3. Equivalent width as a function of effective temperature for all the lines of the multiplet. The equivalent width of Ti I 22274.1 Å has not been plotted since it is almost undiscernable from that of Ti I 22211.2 Å. The thick lines correspond to computations neglecting the formation of molecules, while the thin lines result from calculations taking it into account.

Line profile and contribution function computations show, however, that at typical umbral temperatures the Ti I lines are almost unaffected by the formation of TiO molecules, although the latter are abundant. Fig. 3 shows the equivalent widths of the lines as a function of the effective temperature of the atmospheric models. The non-grey radiative equilibrium models of Kurucz (1991a, b) were employed. These calculations were carried out in the absence of a magnetic field. The thick lines refer to computations ignoring the formation of molecules, while the thin lines represent the case with molecule formation included. As the temperature decreases the influence of molecular TiO increases. The results of the two types of computations begin to diverge only at effective temperatures below approximately 4000 K, however. The reason for the small influence of TiO formation is that the height range at which the Ti I lines are formed has almost no overlap with the higher atmospheric layers at which significant amounts of TiO molecules exist (the TiO appears to collect in the coolest layers of the atmosphere, namely the upper photosphere).

The unnormalized Stokes I line depths (i.e. the depth of the Stokes I profile unnormalized to the continuum intensity) are plotted as a function of the effective temperature in Fig. 4a. Fig. 4b shows a similar plot for the line depths normalized to the continuum intensity. The former representation indicates which temperature structures would dominate the signal when features having different temperatures are present in the same resolution element, while the latter reveals the signal strength to be expected for observations unaffected by stray-light.

Due to the low ionization potential of neutral titanium (6.82 eV), the low excitation potentials and small $\log gf$ values of these lines they show a significant strength only in cool features such as sunspot umbrae and are very sensitive to temperatures above umbral values. At umbral temperatures the line strength is relatively insensitive to T, while at lower temperatures the lines

Fig. 2. a Stokes I profile of Ti I 22310 Å computed using the Kurucz radiative equilibrium model of effective temperature 4250 K, a longitudinal magnetic field strength of 2000 G and no macroturbulent velocity broadening. **b** The contribution function to the Stokes I profile plotted in **a** as a function of wavelength and optical depth at $\lambda = 22000$ Å. **c** Cut through the contribution function surface plotted in **b** at a wavelength at which the contribution function is largest (solid line) versus geometrical *height*. The dashed and dotted lines correspond to similar cuts for the Fe I 15648 Å and Fe I 6302 Å lines, respectively.
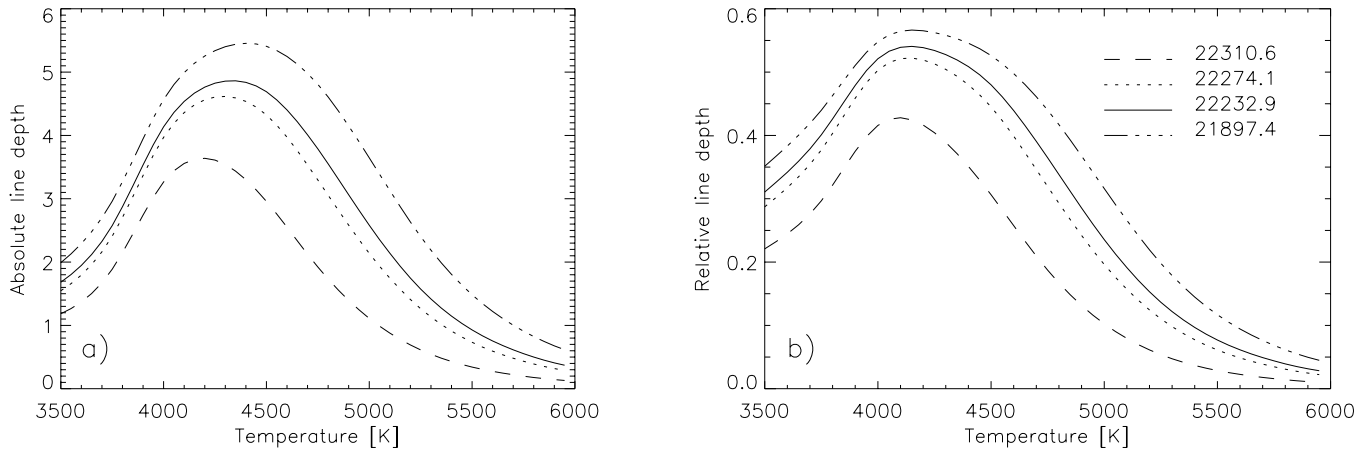
Fig. 4. a Unnormalized Stokes I line depth computed for unsplit line profiles vs. effective temperature. The units on the vertical axis corresponds to $10^8\,\mathrm{erg\,s\,cm^{-2}\,(sr\,\mu m\,s)^{-1}}$. The Kurucz (1991a, b) radiative equilibrium atmospheric models are used. Since the curves for Ti I 22211.22 Å and Ti I 22274.07 Å are almost identical, only one of them is plotted. **b** Same as **a**, but for line depths that have been normalized to the continuum intensity.

become weaker again. Hence, the Ti I lines are ideal for probing umbrae. The weakening at low temperatures is mainly due to the flattening of the temperature stratification at low temperatures (in particular the decreased temperature difference between the heights of continuum and line formation). Note that the equivalent width hardly decreases with decreasing T_{eff} even at low values of T_{eff} (Fig. 3).

2.5. Sensitivity to stray-light

The temperature sensitivity of these lines is one of their great assets. Since they are only prominent in cool features, their profile shapes are practically unaffected by polarized stray-light from the surrounding plage or quiet sun regions, where the lines almost disappear. However, contamination from the colder parts of the penumbra into the umbra, and vice versa, cannot be excluded. It should be noted that at 2.2 μm the continuum contrast between the penumbra and the umbra is strongly reduced relative to the contrast at visible wavelengths. For example, the continuum contrast between a quiet sun atmosphere with $T_{\mathrm{eff}} = 5750$ K and an umbral atmosphere with $T_{\mathrm{eff}} = 4250$ K is 4.3 at 5250 Å while it is only 1.4 at 22310 Å.

Unpolarized stray light (from the quiet sun continuum) still can affect Ti I spectra by decreasing their strength through the addition of a pure continuum component. Spectral stray light also has a similar effect. It is absent in FTS spectra, but provides an unknown contribution to the NIM spectra (Sect. 3). Figs. 3 and 4 allow us to estimate the maximum influence of stray light from, e.g., the quiet sun ($T_{\mathrm{eff}} = 5750$ K) on, e.g., umbral line profiles ($T_{\mathrm{eff}} = 4500$ K). This is given by the ratio of their strength at 5750 K to that at 4500 K, which lies in the range $0.07 - 0.17$ for the unnormalized line depths and in the range $0.04 - 0.08$ for the equivalent widths. This would correspond to a situation in which one half of the signal is originating from the quiet sun and the other from the umbra. Since the straylight will always be smaller than these estimates, we can safely neglect

its influence on the line shape (e.g. any component at the centre of the 22310 Å with a depth $\lesssim 0.02$ is a π-component arising inside the spot).

Unpolarized stray light only affects Stokes I directly, but nevertheless also enters into Stokes V, Q and U via the continuum intensity with which generally all Stokes parameters are normalized. Stray-light contamination reduces the strength of the Ti I lines. Consequently, the influence of the stray light can be mistaken for too high a temperature or too low a filling factor. We stress that it can in no way falsify the values of the magnetic or velocity parameters obtained in the analysis. Nevertheless ratios between lines with different temperature sensitivities have to be used to separate the contribution of the temperature and the filling factor from each other. This can in principle be achieved with a pair of 2.2 μm Ti I lines, since the ratios of their line strengths are somewhat temperature dependent (left panel of Fig. 4). Rather accurate observations are required for this, however.

Consider now the situation typically present within sunspots: Gas at different temperatures is present on small scales (umbral dots within the darker umbral background, bright and dark penumbral filaments). Then the strengthening of the lines with sinking temperatures acts against the decrease in continuum intensity. Whether the cooler or the hotter material contributes most to observations averaging over a certain amount of both temperature components depends on the relative strengths of the two effects and on the relative filling factors of the two components. Due to the strong thermal sensitivity of the continuum in the visible the signals in most lines in this spectral range are dominated by the hotter material. In the case of the 2.2 μm Ti I lines, however, the cooler material invariably dominates for $T_{\mathrm{eff}} \lesssim 4500$ K unless it is only a very minor constituent of the atmosphere. For example, if there are two components, one at 4500 K, the other at 5000 K, each filling half of the spatial resolution element. According to Fig. 4a the warmer component will only contribute $\sim 25\%$ to the depth of the observed profile

Table 2. Summary of the NIM observing sequences

Date	Starting local time	Stokes profile	λ [Å]	Starting airmass	Remark
21 April 1996	17:24:37	V	22211.2	2.98	Slit positioned in the middle of the spot
21 April 1996	17:19:29	Q	22211.2	2.83	Slit positioned in the middle of the spot
21 April 1996	17:14:19	U	22211.2	2.70	Slit positioned in the middle of the spot
21 April 1996	17:06:14	U	22310.6	2.51	Slit positioned in the middle of the spot
21 April 1996	17:00:58	Q	22310.6	2.41	Slit positioned in the middle of the spot
21 April 1996	16:55:15	V	22310.6	2.30	Slit positioned in the middle of the spot
21 April 1996	14:07:54	Q	22310.6	1.16	Scan in the N-S direction
21 April 1996	12:25:45	V	22310.6	1.06	Scan in the N-S direction

of Ti I 22310 Å. If the temperature difference is larger the contribution of the warmer component becomes correspondingly smaller. These calculations therefore suggest that the Ti I lines probe the cool components of the inhomogeneous atmospheres of sunspots.

3. Observations

Two data sets are analysed in this paper. Both have been obtained using the NSO McMath-Pierce telescope on Kitt Peak, but with different spectrographs and detectors.

3.1. FTS observations

The first data set consists of an FTS (Fourier Transform Spectrometer) spectrum recorded on 31st January 1991 in a sunspot umbra (NOAA 6469) at $\mu = \cos\theta = 0.43$. Stokes I and V spectra of all 5 lines of the multiplet were recorded simultaneously. The integration time was 38 minutes and the resolving power 300 000. These observations have been described in more detail by Rüedi et al. (1995).

3.2. NIM observations

The second data set was obtained with the NIM (Near Infrared Magnetograph, Rabin 1994) 256×256 pixel InSb array detector and the main spectrograph. The pixel size of the InSb array is 0.067 Å in the spectral and $0.177''$ in the spatial direction. The region observed was a sunspot born 1 day previously (NOAA 7958). It was located at $\mu = \cos\theta = 0.43$. The slit was oriented in the E-W direction and two different types of observations were carried out:

a) The slit was positioned in the centre of the spot and the complete Stokes vector was recorded sequentially in the two most magnetically sensitive lines of the multiplet. The observing sequence was as follows: Stokes V, Q, U in Ti I 22310.6 Å ($g = 2.5$) followed by Stokes U, Q and V in Ti I 22211.2 Å ($g = 2.0$). The total time needed for this sequence was 35 minutes during which the spot did not appear to undergo major changes. This view is supported by the fact that we obtain good simultaneous fits to the Stokes vector

of both lines in spite of their components being observed in the reverse order. Fig. 6 shows the FPA (focal plane arrays) frames of these observations. The frames on the left correspond to the triplet Ti I 22310 Å ($g = 2.5$), those on the right to Ti I 22211 Å ($g = 2.0$). The FPA frames corresponding to Stokes V, Q and U are depicted from top to bottom. These are the data analyzed in greatest detail in this paper.

b) A scan in the N-S direction (with the slit still oriented in the E-W direction) was performed in Stokes V of Ti I 22310 Å and repeated in Stokes Q. In this case the whole sunspot was scanned. In Stokes V the slit was positioned at 16 different locations separated by $3''$ from each other. In Stokes Q only the first 12 locations of the Stokes V scan were observed (due to instrumental problems).

A summary of these observation sequences is presented in Table 2.

The seeing at the time of the observations was mediocre. Therefore we cannot expect a spatial resolution better than $3''$ and should keep this in mind when interpreting the results. In order to increase the S/N we consequently averaged 10 neighbouring rows of the array detector (corresponding to $1.77''$).

Besides the standard reduction procedure of observations with array detectors, we corrected for telluric line blending (cf. Sect. 4) and for possible spatial shifts of the sunspot's position occuring between the different observations inside one data set. (They were determined by comparing the position of the sunspot along the slit in the intensity images corresponding to Stokes V, Q and U, respectively.) These shifts are small (a couple of pixels at the most) and are probably due to an inexact correction of the solar rotation by the instrumentation.

4. Telluric line blending

Rüedi et al. (1995) showed that the Stokes I spectra of the Ti I lines used in this paper are strongly affected by telluric blends and also demonstrated that they can be easily removed following the procedure originally proposed by Hall (1974) and used by Saar & Linsky (1985). Rüedi et al. (1995) extended this technique to blend removal from polarized Stokes profiles. Here we follow their basic procedure.

For the FTS data we simply used the blend-corrected data of Rüedi et al. (1995). In the case of the NIM data quiet-sun observations of the same wavelength range were recorded just before (Ti I 22310 Å) or after (Ti I 22211 Å) the Stokes V observations of the corresponding lines.[1] Before determining Stokes I and V from the Stokes $I \pm V$ observations, we corrected each of them for the telluric blends according to the formula:

$$(I \pm V)_{\text{spot}} = \frac{(I \pm V)_{\text{obs. spot}}}{(I \pm V)^x_{\text{obs. quiet}}},$$

where $(I \pm V)_{\text{spot}}$ stands for the true solar contribution to the total spectrum observed in the sunspot, $(I \pm V)_{\text{obs. spot}}$. $(I \pm V)_{\text{obs. quiet}}$ corresponds to the quiet sun spectra which have been observed using the same observational setup, and $x =$ (airmass during spot observations)/(airmass during quiet-sun observations). The same procedure was repeated to correct the Stokes Q and U spectra.

Some of the observations were carried out in the late afternoon. At that time, the airmass between two consecutive observations changes considerably. Also, due to the large airmass, errors in determining the airmass are amplified. These spectra may therefore be somewhat under- or overcorrected. An alternative would be to use the airmass averaged over the observing interval. This would account for the non-linear increase of the airmass during an observation late in the day (S. Saar, private communication).

5. Analysis and results: FTS observations

Simultaneous fits to the four lines of the multiplet which are unblended by other solar lines were performed with the inversion code described by Solanki et al. (1992b, 1994), now modified to take into account TiO dissociation equilibrium. Fig. 5 shows the result of such a profile fit. It has been obtained using the radiative equilibrium atmospheric models of Kurucz (1991b), with a height-dependent field strength. On the whole the profile shapes and strengths are very well reproduced. The slightly too strong Stokes I profile obtained for Ti I 22232.9 Å may be due to an uncertainty in the true continuum level. Due to the goodness of these fits, obtained with the literature values of $\log gf$ that are listed in Table 1, we see no need to redetermine the $\log gf$ values. The good fits also indicate that the telluric blends were completely and accurately removed by Rüedi et al. (1995). The code returns a field strength of 2820 G at $z = 110$ km or $\log \tau = -2.15$ ($\lambda = 22000$ Å), corresponding roughly to the height of line formation. A horizontal or vertical distribution of field strength is required to reproduce the data. If no horizontal distribution of the field is assumed to be present, then the magnetic broadening implies a vertical field strength gradient

of 4 G km^{-1} at the level of line formation. Finally, a Gaussian micro- and macroturbulent broadening velocity of 1.0 km s^{-1} and 1.8 km s^{-1}, respectively, was also needed. The temperature of the atmospheric models corresponds to an effective temperature of 4340 K.

For the fit shown in Fig. 5 the inversion code returned a magnetic filling factor of unity or equivalently an absence of stray-light. Therefore, the temperature obtained from the inversion corresponds to an upper limit. A higher temperature would be unable to produce profiles of the required strength (c.f. Fig. 3). At lower filling factors (and correspondingly lower umbral temperatures) the fits are of lower quality, the depths of the different lines not being reproduced properly. As pointed out in Sect. 2.5 the ratios between the Ti I lines possess a certain temperature sensitivity due to the slightly different behaviour of their line depths and equivalent widths (Figs. 3 and 4). Consequently, we estimate the determined temperature to be accurate within $\pm$ 100 K.

Inversions were carried out using two different groups of atmospheric models: the non-grey radiative equilibrium models of Kurucz (1991a, b) and the empirical umbral models of Maltby et al. (1986). Good fits could be achieved with both types of models. The quality of the fit depends very strongly on the inclination angle of the magnetic field relative to the solar surface, however, even though only Stokes I and V are involved. (The combined effects of the filling factor and inclination angle subtly influence the line profiles. Therefore, depending on the starting value of the inversion procedure for these two parameters, different minima in χ^2-surface may be reached. This problem was noticed and overcome using many different starting values.) [2]

6. Analysis and results: NIM observations

6.1. E-W cut

The observed sunspot was part of a relatively newly emerged bipolar active region near the west limb. It consisted of the observed sunspot, located on the limbward side of the active region and of a group of pores of opposite polarity located on the disc centre side. Fig. 6 shows the Stokes V/I_c, Q/I_c and U/I_c observations of the two most magnetically sensitive lines of the multiplet (NIM data set 'a', cf. Sect. 3.2). The spectrograph slit was aligned in the East-West direction, so that the top of each frame points to the solar limb while the bottom points to the pores of opposite polarity. The centre of the spot is located approximately at row number 160.

Some interesting features can be seen in Fig. 6. Firstly, the strongly split Stokes Q component is spatially well localised (in the sunspot umbra). It ends quite abruptly, with almost no decline of the observed magnetic field strength toward the sunspot boundaries. On the Stokes V frames a second, weakly split component is also visible. Its appearance outside of the sunspot is very homogeneous and it can be traced back all the way into

---

[1] During the observations, we paid attention that the umbral and quiet sun spectra correspond approximately to the same longitude in order to avoid possible shifts of the solar lines with respect to the telluric lines due to solar rotation. Since no solar lines are known to blend the lines we are interested in and since the latter almost disappear in the quiet sun, such precautions were probably superfluous.

[2] Note that in the preliminary results presented in Rüedi et al. (1997), it was not realised how critical this parameter is, and it was therefore not properly taken into account.
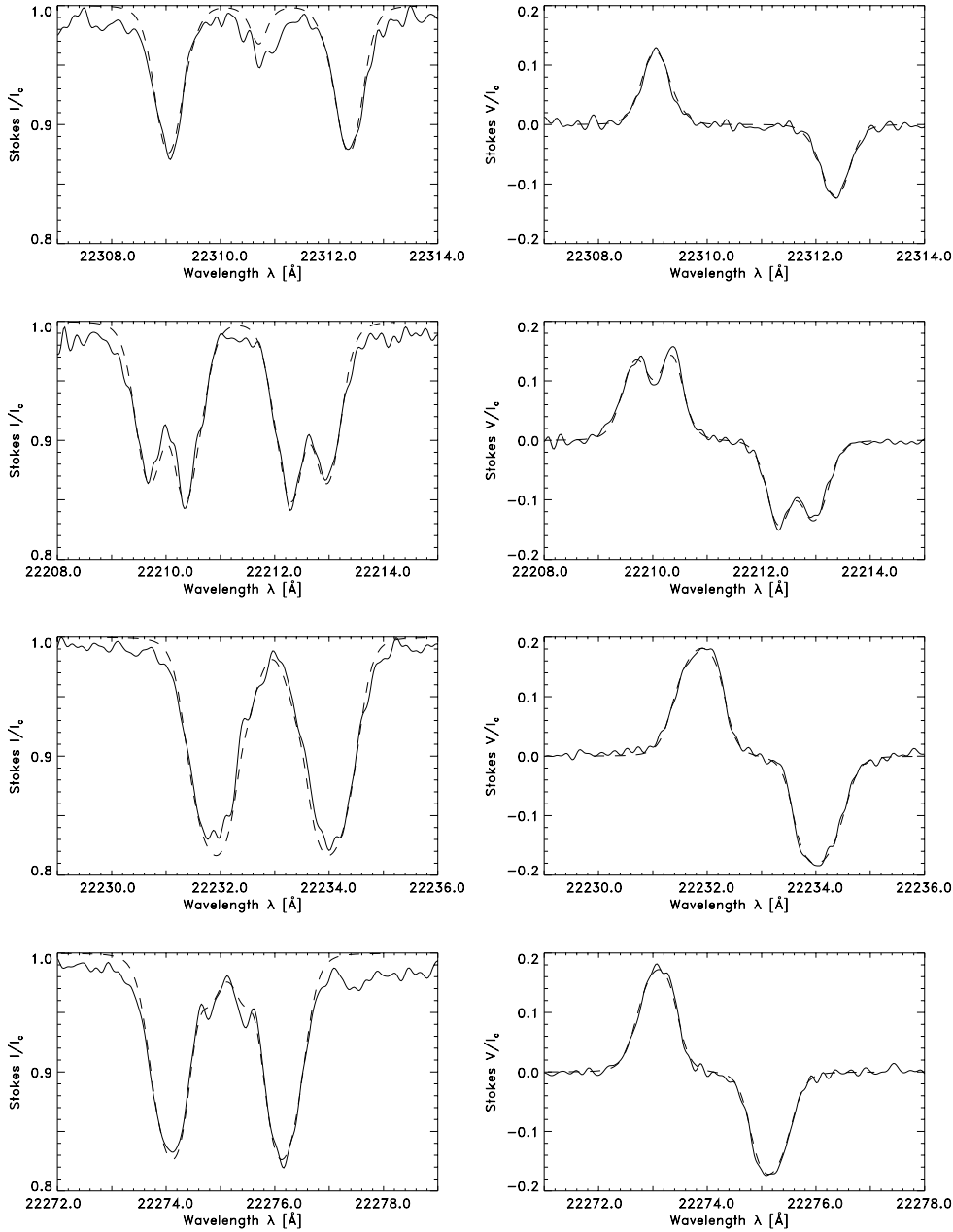
Fig. 5. Stokes I (left) and V (right) FTS spectra of the four Ti I lines around 2.2μm which are unblended by solar lines. These recordings were made in a large sunspot umbra. The solid curves represent the observations (after telluric blend correction), the dashed curves the best fit obtained using Kurucz (1991a, b) models. The continuum level of the observations was determined by considering a larger wavelength interval.

the umbra where the splitting of the strong component is largest, although it disappears in the central part of the umbra. The weak component also remains visible all the way to the pore group. The Stokes V profile appears to show distinct magnetic components, with only faint signs of intermediate splitting. This contrasts strongly with the spatial variation of the Zeeman splitting exhibited by most other spectral lines in sunspots.

In the following we present a quantitative analysis of the Ti I data using inversions.

Fig. 7 shows the observed Stokes V and Q line profiles (solid lines) corresponding to position 160 of Fig. 6, located within the umbra. The peculiar shape of the Stokes Q profile of the Ti I 22211 Å line is due to its unusual splitting pattern (cf. Fig. 1). The dashed lines represent the fits. The relatively poor quality

of the fit to the Stokes V profile strengths is probably due to an inadequate correction of the telluric line blends. Again, as mentionned in Sect. 4, our correction procedure may be improved by using the airmass averaged over the observation interval. The shape of the Stokes V profile of the Ti I 22211 Å line suggests that it has been undercorrected for telluric line blending. This is not surprising since Stokes V of Ti I 22211 Å was observed late in the day, at a time when the airmass was changing very rapidly. A larger correction would produce a profile of stronger intensity and would allow a better simultaneous fit to both lines. We prefer, however, to simply use the airmass corresponding to the central time of the observations, rather than consider it as a free parameter. Part of the discrepancy between observed and best fit profiles might also be due to the fact that we modelled
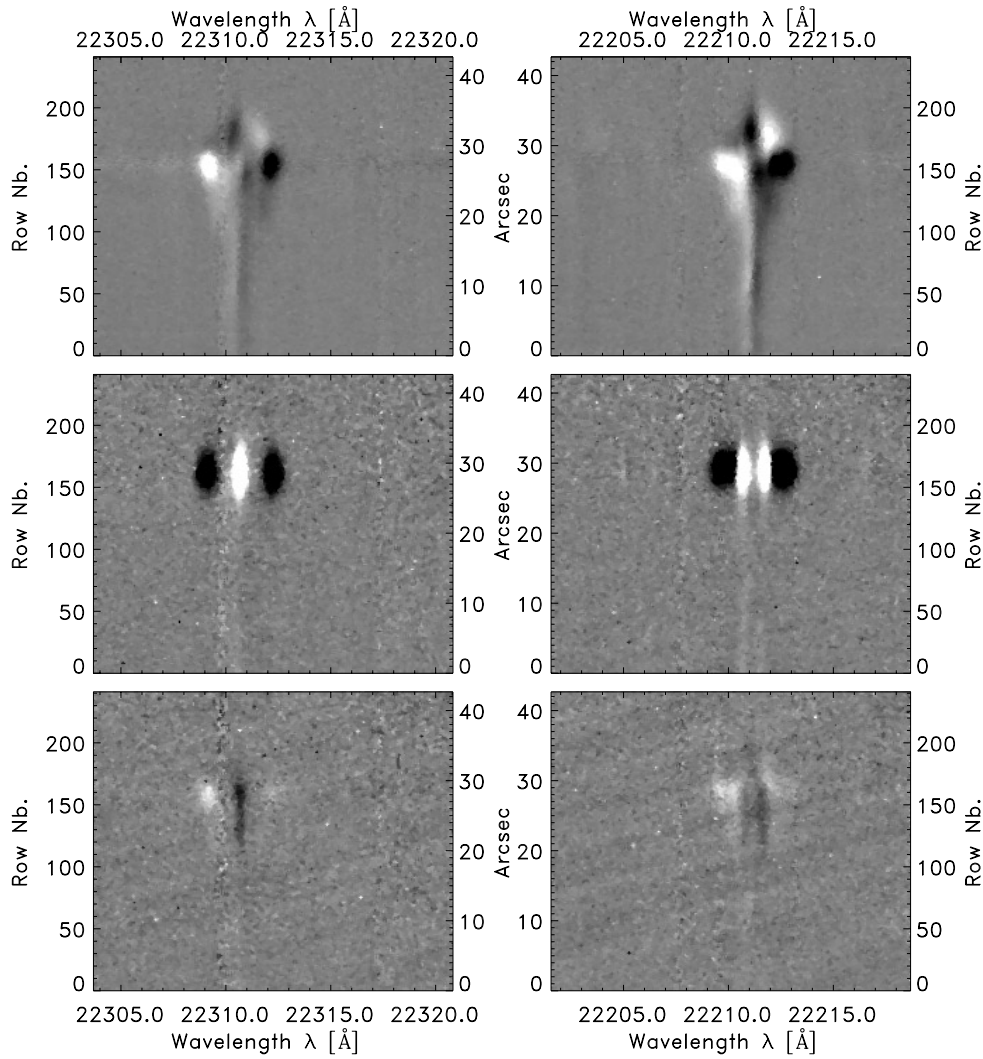
Fig. 6. East-West cut through the sunspot centre. From top to bottom: FPA frames of Stokes V/I_c, Q/I_c and U/I_c observed with NIM. The frames on the left depict the Ti I 22310.6 Å ($g = 2.5$) line, those on the right the Ti I 22211.2 Å ($g = 2.0$) line. The vertical stripe of enhanced noise between the π- and the blueward σ-component of the $g = 2.5$ line corresponds to the location of a telluric absorption feature.
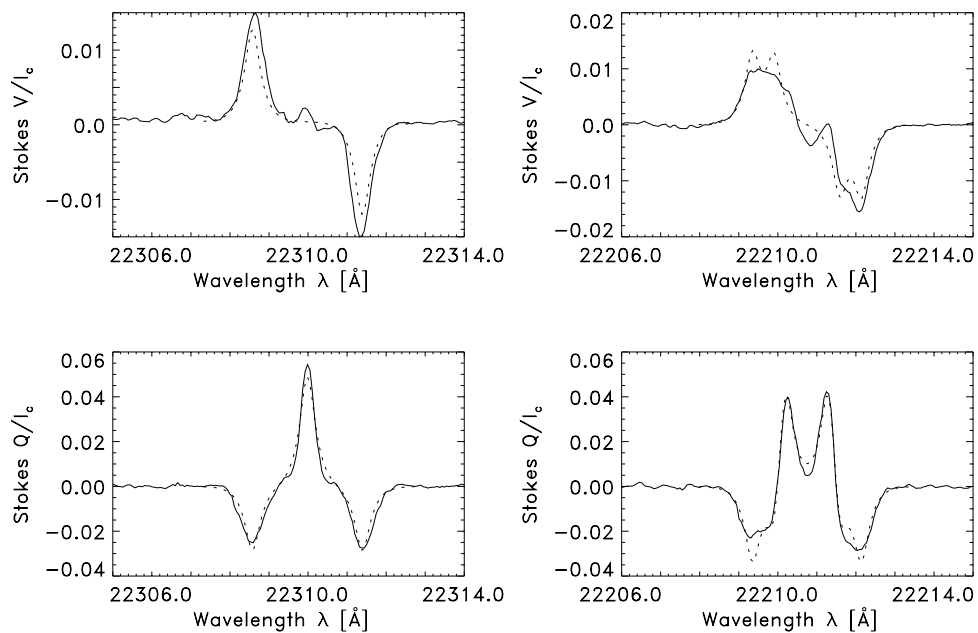

Fig. 7. Typical fit obtained to Stokes V (top) and Q (bottom) NIM spectra. The plotted spectra correspond to spatial position 160 on the FPA frames (Fig. 6). Stokes U is dominated by noise and has consequently not been plotted

this profile using only one magnetic component. The small inversion in the middle of both Stokes V line profiles suggests the presence of a second magnetic component (possibly magnetic stray light from the penumbra).

Fig. 8 summarizes the results of the inversion of all the profiles of Fig. 6 showing a polarized signal. The inversions were carried out with either one or two magnetic components (cf. Bernasconi & Solanki 1996). The values on the horizontal axis refer to the row number on the array detector (they correspond to the values given on the vertical axis of Fig. 6). The numbers increase towards the solar limb. The point at pixel position 107, separated from the others by the vertical dashed line, represents the parameters of the fit to the Stokes profiles averaged over the first 100 rows of the detector. These rows showed weak signals of similar amplitudes and splittings. Fig. 8a exhibits the continuum intensity of the observed spectra in arbitrary units. Figs. 8b-e show the magnetic field strength, B, the inclination angle of the magnetic vector to the normal to the solar surface, i.e. zenith angle, ζ, the azimuth, χ ($\chi = 0$ means that the magnetic vector points to the west, i.e. roughly toward the limb), and the Doppler velocity shift along the line of sight. Fig. 8f displays a measure of the Stokes I line strength in arbitrary units. The plus signs stand for the magnetic component having a strong magnetic field strength, while the diamonds correspond to the weak magnetic field strength component.

In the darkest parts of the umbra, the profiles were reasonably reproduced with just one magnetic component. Its field strength reaches 2700 G and does not show much variation in the umbra itself. It can be followed outside the purely umbral region where its strength decreases somewhat. On the whole this component is not much inclined to the vertical. It is most inclined on the solar limb side, where it reaches values around 60°. Intrinsic velocity shifts of this component are not observed.

The second magnetic component has a considerably lower field strength. On the limbward side of the penumbra, the field strength ranges between 700 G and 950 G, while on the discward side only an upper limit of 500 G can be set. This component is much more horizontal than the strong-field component. The azimuth associated with these weaker field components differs by roughly 180° between the limbward and discward sides of the penumbra. (Due to the change in sign of the Stokes V profile between the limbward and the discward side of the penumbra, there is little ambiguity in this azimuth.) Furthermore, the weak-field component shows large velocity shifts relative to the strong-field component, which are compatible with the signature of the Evershed effect.

At this point it is important to remember that the seeing at the time of the observations was mediocre. The homogeneity of the values relating to each component separately (strong-field component, weak-field component on the limb side and weak-field component on the disc-centre side) suggests that our data are affected by stray light from one component into the other (probably due to the poor seeing conditions). Fig. 8f shows a relative measure for the strength of the Stokes I line profiles relating to each component. The strong-field component is localised in the umbra and decreases steadily outwards, where it

contributes only a small amount to the composite profiles. Such a behaviour is fully consistent with the stray-light hypothesis. Judging from these observations alone it is not absolutely clear to which extent one or two components are really present in a given resolution element. It is, however, quite clear that there is no gentle decrease of the field strength, or gradual increase of ζ as we move from the centre of the sunspot to its periphery.

6.2. N-S Scan

Fig. 9 presents results obtained from the NIM data set 'b'. The slit was again positioned in the E-W direction and the sunspot was scanned in the N-S direction. This data set contains only Stokes V and Q measurements of the Ti I 22310 Å line. Furthermore, the Stokes Q measurements only extend from position 1 to 12 and were recorded approximately 100 minutes after the Stokes V measurements. Due to possible sunspot evolution, pointing drift or inaccurate compensation of the solar rotation during this period, we fitted Stokes V and Q separately and determined only the magnetic field strengths and velocity shifts. The returned values of these free parameters are independent of the prescribed ζ, χ, etc. This was done along three different slices directed roughly N-S. The numbers along the x-axis increase from north to south. The distance between two slit positions is $3''$.

The slice nearest to the limb (top row of Fig. 9) is bow shaped and curves around the umbra. A bow shaped slice was prefered to a straight one in order to sample the penumbra over as large N-S a distance as possible without contamination from the umbra. Along this slice the Stokes Q signal was very weak and only Stokes V was fit. At positions 1, 2 and 16 the Stokes V profiles were either complex or too weak to be fitted.

The slice lying furthest from the limb (lowest frame in Fig. 9) is also bow shaped, with the opposite curvature as the first slice (for the same reasons). This slice does pass partly inside a secondary umbra however. Again, only Stokes V was fit, because Stokes Q was weak. Note the larger field strength and the small velocity shifts in the (secondary) umbra.

Finally, the central slice is a straight N-S slice passing through the centre of the umbra. In this case both Stokes Q and V profiles, which give similar results, were present in the umbra (strong-field component). Fits to Stokes Q are denoted by '+'-signs, those to Stokes V with stars in Figs. 9c and d (middle row). In the penumbra, where the magnetic field is weak this slice lies at the polarity inversion, so that the Stokes V profiles are small with complex shapes and only Stokes Q is fit. At slit positions passing through the umbra only the strong-field component could be clearly discerned in Stokes Q (cf. Fig. 6). It is represented by "+"-signs in the central panels of Fig. 9. The sudden drop in the magnetic field strength observed in Stokes Q along this slice is accompanied by a sudden change in the inclination angle of the magnetic field vector. This appears in the data as a sudden change in the sign of Stokes Q which is compatible with a change in inclination from nearly vertical in the umbra to nearly horizontal in the penumbra. This sudden change in the inclination accompanied by a sharp drop of the
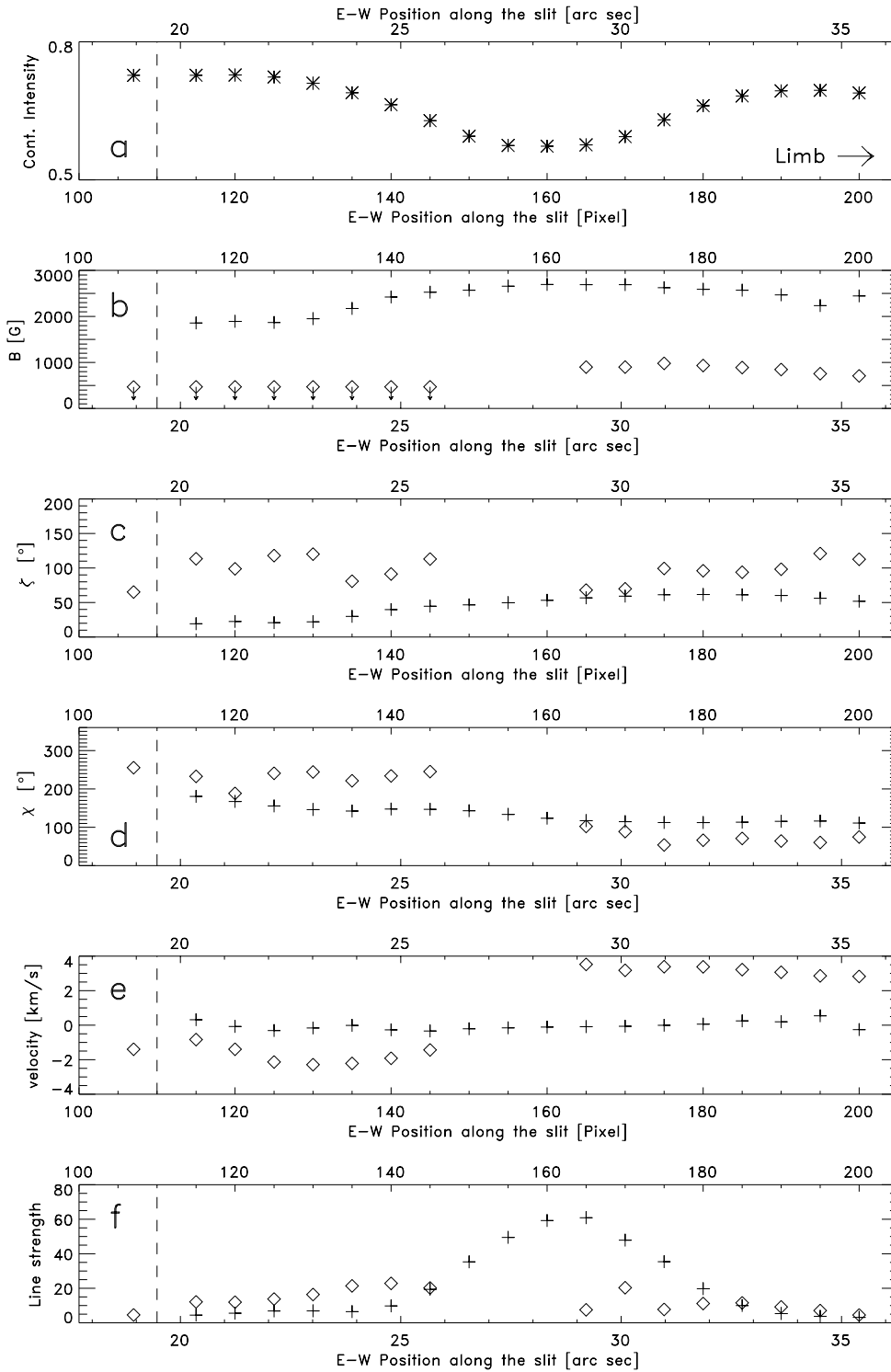
Fig. 8a–f. Parameters of the fit to the FPA spectra shown in Fig. 6. The slit was oriented in the E-W direction and runs through the centre of the umbra. The "+"-signs represent the strong magnetic component, while the diamonds stand for the weak magnetic field component. The point at pixel position 107, separated from the others by the vertical dashed line, represents the parameters of the fit to the Stokes profiles averaged over the first 100 rows (18″) of the detector. **a:** the continuum intensity of the spectra in arbitrary unit, **b:** the magnetic field strength, B, **c:** the inclination angle to the normal of the solar surface, i.e. zenith angle, ζ, **d:** the azimuth, χ (in local solar coordinates; $\chi = 0$ points to the west), **e:** the Doppler velocity along the line of sight in km/s, velocity, **f:** Line strength in arbitrary units.

magnetic field strength is in good agreement with the results plotted in Fig. 8. In addition, in Fig. 9 we again observe little gradual variation of the magnetic field strength as a function of the position, but rather abrupt changes. This strongly suggests that the strong-field magnetic component is localised in the umbra while the weak component belongs to the penumbra and superpenumbral canopy. Since the projected N-S extent of

the sunspot is much larger than its projected E-W extent, seeing influences the results much less in Fig. 9 than in Fig. 8.

We see no substantial velocity shift in the kilogauss components, but observe velocity shifts compatible with the Evershed effect in the weaker field components. As expected, these velocity shifts decrease as a function of distance from sunspot centre as measured parallel to the solar limb. This is in agreement with
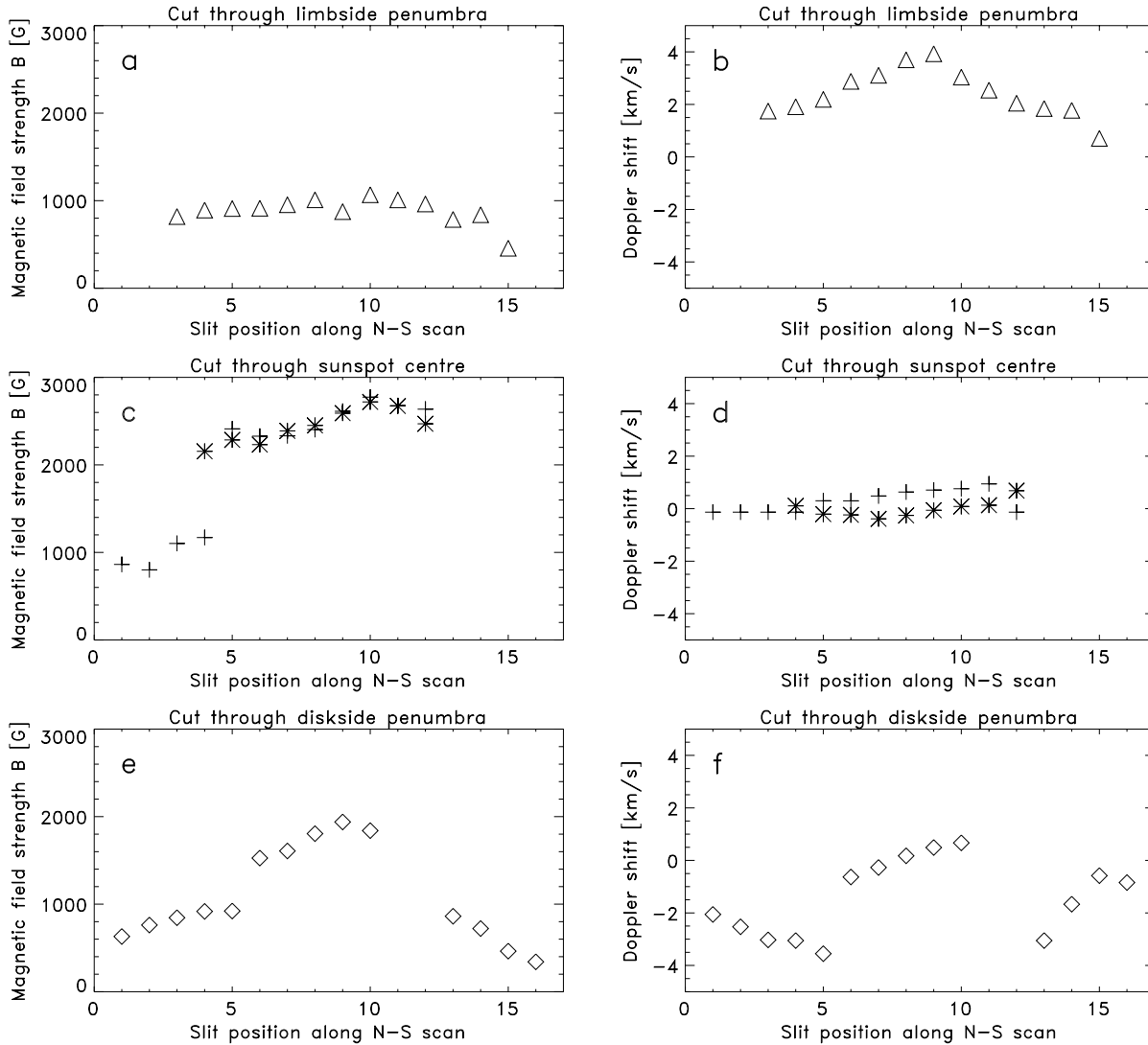
Fig. 9a–f. Plot of the magnetic field strength, B (left) and of the Doppler shift along the line of sight (right) for three different cuts through the sunspot in the N-S direction (position 1-16). The top and bottom rows refer respectively to the values obtained from fits to the Stokes V profiles in the limbward and diskward side of the penumbra. On the discward side the cut passes through an outer secondary umbra at slit position 6-10. The central row refers to a cut through the sunspot centre, where both Stokes V and Q observations are available. The "+"-signs refer to values obtained from fits to the Stokes Q profiles, while the stars refer to the Stokes V profiles.

the hypothesis of a velocity directed radially outwards along the solar surface in a roughly circular sunspot. The weak field component, seen in Stokes Q along the central slice, is compatible with the weak fields observed in the limbward and diskward part of the penumbra. The absence of a velocity shift in the central slice is also compatible with a radial outflow, which is directed perpendicular to the line of sight at this position.

In summary, no substantial shifts are associated with the kilogauss fields, while weak fields in general exhibit strongly shifted line profiles.

6.3. Weak-field homogeneous component

The weak-field component present practically everywhere outside the sunspot between the spot and the pore group is very

homogeneous over the whole distance of $18''$ seen in the lower parts of the FPA frames plotted in Fig. 6. Its magnetic field strength is not larger than $500\,\mathrm{G}$ and it appears to harbour a line-of-sight velocity directed toward the observer with a magnitude of approximately $1.4\,\mathrm{km\,s^{-1}}$ relative to the umbral component. The same feature is seen in all the frames of the N-S scan with no significant variation of the Doppler shift as a function of the position.

The most natural explanation of this component is that it represents the superpenumbral magnetic canopy and the line shift is the continuation of the Evershed effect in the canopy (see Solanki et al. 1994 for similar results obtained with the $1.56\,\mu\mathrm{m}$ line). The fact that we observe no significant variation of the Doppler shift or of the magnetic flux along the N-S scan is probably due to the configuration of the active region. We

are averaging over a very large area ($18''$) due to a combination of the seeing and the averaging over many spatial positions in order to enhance the S/N.

Since the observed active region was developing, the alternative explanation is that this magnetic field corresponds to emerging flux. Our observations do not allow us to distinguish uniquely between these possibilities, although the constant blueshift of 1.4 km s^{-1} is difficult to explain in the second scenario. A contribution from plage magnetic field to this component is not expected since the Ti I lines are extremely weak in such hot regions. Furthermore plage and network fields would be vertical whereas the component we observe in Ti I is nearly horizontal.

7. Discussion

In contrast to earlier observations (e.g., Beckers & Schröter 1969, Wittmann 1974, Kawakami 1983, Deming et al. 1988, Adam 1990, Lites & Skumanich 1990, McPherson et al. 1992, Solanki et al. 1992b, Keppens & Martinez Pillet 1996), we do not observe a smooth decrease of the magnetic field strength through the umbra and penumbra, but rather an abrupt transition between the strong- and weak-field components.

– One possible explanation of this peculiarity is that the structure of the observed sunspot is unusual and therefore does not match earlier results. This might be the case since this is a young sunspot. However, we find no other evidence supporting such an explanation. In particular, the sunspot showed no obvious sign of evolution during the Ti I observations. However, the sunspot most probably evolved somewhat earlier in the day.

– Another possibility is that earlier observations are more affected by stray light. Due to the strong dependence of the continuum intensity on temperature this could account for discrepancies obtained with sunspot observations carried out in the visible spectral range (Keppens & Martínez Pillet 1996). However, this effect is much reduced in the infrared and cannot account for the discrepancy relative to other infrared measurements, which also exhibit a smooth variation of field strength and inclination (e.g. Deming et al. 1988, McPherson et al. 1992, Solanki et al. 1992b, Hewagama et al. 1993).

– A final possibility is that sunspots are composed of hot and cold components which are mixed on scales below the spatial resolution. Since most spectral lines used for sunspot magnetic field studies are not particularly temperature sensitive, they reveal either the hotter component or some mixture of the two. However, temperature-sensitive spectral lines, such as the Ti I lines used here, preferentially probe the cooler components (see Sect. 2.4).

The current observations do not on their own allow us to distinguish between these 3 possibilities. The combination with Fe I 1.5648 μm spectra is expected to provide more clarity. This is the subject of a separate paper.

The infrared Ti I lines have advantages relative to the visible Ti I lines which have also been used to compare the bright and dark structures of sunspot penumbrae (Stellmacher & Wiehr 1980, 1981, Brants & Zwaan 1982, Wiehr et al. 1984). Due to

their larger wavelength, the Zeeman splitting of infrared lines is much larger and these lines are therefore much more sensitive to magnetic fields. The continuum contrast between dark and bright structures is greatly reduced in the infrared giving a much larger relative weight to the dark structures in low spatial resolution infrared spectra.

8. Conclusions

In the present paper we have studied the properties of the Ti I lines around 2.2 μm relevant for the investigation of solar magnetic features. The combination of large Zeeman splitting and high temperature sensitivity makes them ideal probes of the cool components of sunspots.

We have also carried out the first radiative transfer calculations of these lines and have shown that the influence of TiO formation becomes important only at low temperatures (T$_{\text{eff}} \lesssim 4000$ K, e.g. in the dark parts of umbrae). The calculated Ti I lines reproduce FTS observations of these obtained in a sunspot umbra extremely well.

Finally, we present and analyse (by fitting with synthetic line profiles) Stokes spectra observed at different positions in a young sunspot near the solar limb.

Our observations suggest that the cool structures in the observed sunspot are of two kinds. On the one hand, we observe a fairly vertical component associated with the umbra (zenith angle $\lesssim 50°$). It possesses a large magnetic field strength that shows little scatter around its mean value of 2500 G. On the other hand, we also observe a weak-field component ($B \lesssim 1200$ G) located in the penumbra which is much more horizontal (zenith angle between $70°$ and $120°$) and shows the signature of a strong Evershed effect (line-of-sight velocity up to 3.5 km s^{-1}). There appears to be little cool material at intermediate field strengths. The Evershed flow is restricted to the cold horizontal filaments.

Finally, our observations reveal a weak homogeneous magnetic component extending all the way between the observed sunspot and the neighbouring pore group of opposite polarity. This component has a low field strength (≤ 500 G) and shows a small blueshift relative to the umbral magnetic component. We interpret this component as the superpenumbral canopy and the associated velocity as the continuation of the Evershed effect. These observations provide the first evidence for cool gas in the canopy of sunspots.

References

Adam M.G., 1990 Solar Phys.125, 37
Beckers J.M., Schröter E.H., 1969 Solar Phys. 10, 384
Bernasconi P.N., Solanki S.K., 1996 Solar Phys. 164, 277
Biémont E., 1976 A&AS 26, 89

Brants J.J., Zwaan C., 1982 Solar Phys. 80, 251

Deming D., Boyle R.J., Jennings D.E., Wiedemann G., 1988 ApJ 333, 978

Grossmann-Doerth U., Larsson B., Solanki S.K., 1988 A&A 204, 266

Hall D.N.B., 1974 *An Atlas of Infrared Spectra of the Solar Photosphere and of Sunspot Umbrae* Kitt Peak National Observatory, Contribution No. 556, Tucson, AZ.

Hewagama T., Deming D., Jennings D.E. et al., 1993 ApJSS 86, 313

Kawakami H., 1983 PASJ 35, 459

Keppens R., Martínez Pillet V., 1996 A&A 316, 229

Kurucz R.L., 1991a, in: Stellar Atmospheres: Beyond Classical Models L. Crivellari, I. Hubeny, D.G. Hummer Kluwer, Dordrecht, p. 441

Kurucz R.L., 1991b, in: Precision Photometry: Astrophysics of the Galaxy A.G. Davis Philip, A.R. Upgren, K.A. JanesL. Davis Press, Schenectady

Lites B.W., Skumanich A., 1990 ApJ 348, 747

Maltby P., Avrett E.H., Carlsson M. et al., 1986 ApJ 306, 284

McPherson M.R., Lin H., Kuhn J.R., 1992 Solar Phys. 139, 255

Mihalas D., 1967 *Methods in Comp. Phys. 7* 1

Rabin D., 1994 in: Infrared Solar Physics D. Rabin, J. Jefferies, C.A. Lindsey Kluwer, Dordrecht IAU Symp. 154, 449

Rüedi I., Solanki S.K., Livingston W., Harvey J.W., 1995 A&ASS 113, 91

Rüedi I., Solanki S.K., Livingston W., 1997, in: 1st Advances in the Physics of Sunspots Euroconference, Advances in the Physics of Sunspots B. Schmieder, J.C. del Toro Iniesta, M. Vázquez Astron. Soc. Pacific Conf. Ser. Vol. 118, p. 237

Saar S.H., 1996a, in: Stellar Surface Structure K.G. Strassmeier, J.L. LinskyKluwer, Dordrecht, IAU Symp. 176, 237

Saar S.H., 1996b, in: Magnetodynamic Phenomena in the Solar Atmosphere – Prototypes of Stellar Magnetic Activity, Y. Uchida, T. Kosugi, H.S. Hudson Kluwer, Dordrecht, IAU Coll. 153, 367

Saar S.H., Linsky J.L., 1985 ApJ 299, L47

Solanki S.K., 1987, *Ph.D. Thesis* No. 8309, ETH, Zürich

Solanki S.K., Rüedi I., Livingston W., 1992a A&A 263, 312

Solanki S.K., Rüedi I., Livingston W., 1992b A&A 263, 339

Solanki S.K., Montavon C.A.P., Livingston W., 1994 A&A 283, 221

Stellmacher G., Wiehr E., 1980 A&A 82, 157

Stellmacher G., Wiehr E., 1981 A&A 103, 211

Wallace L., Livingston W., 1992 *An Atlas of a Dark Sunspot Umbral Spectrum from 1970 to 8640 cm^{-1} (1.16 to 5.1 μm)* NSO Techn. Rep. 92–001, National Solar Obs., Tucson, AZ

Wiehr E., Koch A., Knölker M., Küveler G., Stellmacher G., 1984 A&A 140, 352

Wittmann A.D., 1974 Solar Phys. 36, 29